

Spatiotemporal superposed rogue-wave-like breathers in a $(3 + 1)$ -dimensional variable-coefficient nonlinear Schrödinger equation*

Hai-Ping Zhu^a, Ya-Jiang Chen^b

^aCollege of Ecology, Lishui University,
Lishui, Zhejiang, 323000, China
zhp63521@126.com

^bCollege of Engineering and Design, Lishui University,
Lishui, Zhejiang, 323000, China

Received: May 4, 2014 / **Revised:** August 12, 2014 / **Published online:** November 18, 2015

Abstract. A one-to-one relation between a variable-coefficient $(3 + 1)$ -dimensional nonlinear Schrödinger equation with linear and parabolic potentials and the standard nonlinear Schrödinger equation is presented, and then superposed rogue-wave-like breather solution is obtained. These explicit expressions, describing the evolution of the amplitude, width, center and phase, imply that the diffraction, nonlinearity and gain/loss parameters interplay together to influence evolutionary characteristics above. Moreover, the controllable mechanism for fast excitation, maintenance, restraint and recurrence of breather is studied. We also provide an experimental scheme to observe these phenomena in future experiments.

Keywords: nonlinear Schrödinger equation, spatiotemporal superposed rogue-wave-like breathers, controllable mechanism.

1 Introduction

The investigation of soliton solutions for nonlinear evolutionary equations [6, 24] is an essential and important issue in nonlinear science. As a ubiquitous and significant nonlinear evolutionary model, nonlinear Schrödinger equation (NLSE) appears in various fields of physics and engineering from nonlinear optics [36], plasmas [33], fluid dynamics [25] to Bose–Einstein condensations (BECs) [27]. Abundant structures of NLSE, such as light bullets [11], solitons [36], similaritons [10], rogue waves [37] and breathers [12] etc., play important roles in many branches of physics.

Among these structures, rogue waves (RWs, also known as freak waves, monster waves and extreme waves) from ocean sometimes can be more times higher than the

*This work was supported by the National Natural Science Foundation of China (grant No. 11375079).

average wave crests. The rational solution (also called Peregrine soliton [26]) of NLSE is the most common prototype to describe the dynamics of RWs. RW events appear from nowhere and disappear without a trace [1]. RWs in higher-order NLSE were also discussed [3]. Akhmediev et al. reported how to excite a rogue wave [2]. Experimentally, Solli et al. [32] reported a randomly created optical rogue wave in a photonic crystal fiber. Dudley et al. [15] investigated the harnessing and control of optical rogue waves in supercontinuum generation. Chabchoub et al. [4] observed rogue wave in a water wave tank. These processes in ocean and nonlinear optics need the controllable RWs, thus many authors theoretically investigated the controllable behaviors of RWs. The management and control of self-similar picosecond [8, 34] and femtosecond [13] RWs has been discussed respectively. Moreover, controllable RW triplets have been reported [7].

However, all investigations above based on the theoretical analysis to rational solutions [7, 8, 13, 34]. In fact, besides the rational solution, breather [12] (periodic in time or space and localized in space or time) is also regarded as a potential prototype to describe the possible formation mechanisms for RWs. Breather solutions have played vital roles in the electronic, magnetic, vibrational and transport properties of the systems. Recently, researchers have also found breathers in the experiments [14, 18]. Analytical and numerical evidence has also demonstrated that the management of breathers can be achieved [23]. Therefore, controlling and making use of breathers are also needed.

All controllable behaviors for RWs based on rational solutions are studied in $(1+1)$ -dimensional (1D) cases [7, 8, 13, 34]. Rational solutions are some special cases of breather solutions [19]. The real world is higher dimensional case, thus direct knowledge of the control for RWs, especially based on breathers, in higher dimension would be more helpful in terms of understanding the physical phenomena related to RWs. Although Yan et al. [35] and Ma et al. [22] studied dynamical behaviors of 3D RWs, they have not discussed the important controllable behaviors of RWs, which will be investigated here. The novelty of this paper lies in: (i) Spatiotemporal superposed breather solution built from first-order and second-order RWs is firstly obtained, and (ii) the manipulation for higher dimensional RWs based on breathers such as fast excitation, maintenance, restraint and recurrence is firstly reported.

In this work, we consider the 3D variable-coefficient (vc) NLSE with linear and parabolic potentials

$$iu_t + \frac{\beta(t)}{2}\Delta u + \chi(t)|u|^2u + V(t, x, y, z)u = i\gamma(t)u, \quad (1)$$

where $u(t, x, y, z)$ is the order parameter in BECs or the complex envelope of the electrical field in optical communication, t denotes time for BECs or propagation distance in a nonuniform single-mode fiber, $\Delta = \partial_x^2 + \partial_y^2 + \partial_z^2$ is the three dimensional Laplacian. The functions $\beta(t)$, $\chi(t)$ and $\gamma(t)$ stand for the diffraction, nonlinearity and gain/loss coefficients, respectively. Potential $V = V_1(t)(x + y + z) + V_2(t)Y^2$ with the strength of the linear and parabolic potentials $V_1(t)$ and $V_2(t)$, and $Y^2 = x^2 + y^2 + z^2$. It is strictly assumed that $V_1(t)$ and $V_2(t)$ are not zero, otherwise, Eq. (1) is back to the 3D NLSE in [11, 21, 28, 29].

2 Superposed RW-like breather solution

At first, we construct one-to-one correspondence between u in Eq. (1) and U in Eq. (5) as follows:

$$u = \frac{\sqrt{l_2}}{W} \sqrt{\frac{\beta}{\chi}} U(T, X) \exp[i\phi(t, x, y, z)], \quad (2)$$

where the similarity variable, width, center, accumulated time and phase:

$$X = \frac{\xi - \xi_c}{W(t)}, \quad W(t) = \frac{3\chi \exp(2\Gamma)}{\beta},$$

$$\xi_c(t) = -l_1 W(t) \int_0^t \frac{\beta(\tau)b(\tau)}{W(\tau)} d\tau, \quad T = \int_0^t \frac{l_2 \beta(\tau)}{W^2(\tau)} d\tau, \quad (3)$$

$$\phi = \frac{W_t}{2\beta W} Y^2 - b(x + y + z) - \frac{3}{2} \int_0^t \beta(\tau)b^2(\tau) d\tau \quad (4)$$

with $\xi = px + qy + rz$, $\Gamma(t) = \int_0^t \gamma(\tau) d\tau$, $l_1 = p + q + r$ and $l_2 = p^2 + q^2 + r^2$. Via this relation, Eq. (1) can be transformed into the traceable NLSE

$$iU_T + \frac{1}{2}U_{XX} + |U|^2U = 0. \quad (5)$$

Moreover, function $b(t)$ and system functions $V_1(t)$, $V_2(t)$, $\beta(t)$, $\chi(t)$ and $\gamma(t)$ satisfy

$$V_1 = -b_t - b \left(2\gamma + \frac{\chi_t}{\chi} + \frac{\beta_t}{\beta} \right), \quad V_2 = \frac{\beta W_{tt} - \beta_t W_t}{2\beta^2 W}. \quad (6)$$

Note that this relation (2) with solutions of Eq. (5) includes many known solitonic solutions in [11], [21, 28, 29]. Without external potentials, we have $W = 1 + 2a_0 \int_0^t \beta d\tau$, and the last expression of Eq. (3) is Eq. (23) in [11] when t and z are exchanged here. When $V_1 = 0$, choosing $W(t) = \exp(2 \int_0^t \beta a d\tau)$ here yields solution expressed as (5) in [21]. If $W(t) = (1 + Ce^{pt}) / [(1 + C)e^{pt/2}]$, solutions in [28] can be regained. When $V_2 = 0$, Eq. (3) gives the value α in solution expressed as (17) and (18) in [29]. Also note that the similarity transformation (2) here is different from that in [22]. Here U is a complex function satisfying the complex NLSE (5), while variables P and Q in [22] are both real functions in the rational forms. Moreover, phase ϕ has different form compared with that in [22].

In the following, we focus on new type of breather for Eq. (1). Via relation (2) and Darboux transformation (DT) method [19] for Eq. (5), an analytical expression for breather solution for Eq. (1) reads

$$u = \frac{\sqrt{l_2}}{W} \sqrt{\frac{\beta}{\chi}} \left[1 + \frac{G + iH}{F} \right] \exp(i\Phi), \quad (7)$$

where

$$\begin{aligned}
\Phi &= \left(1 - \frac{v^2}{2}\right)(T - T_0) + v(X - X_0) + \phi, \\
G &= -k_{12} \left[\frac{k_1^2 \delta_2 \cosh(\delta_1 T_{s1}) \cos(k_2 X'_{s2})}{k_2} - \frac{k_2^2 \delta_1 \cosh(\delta_2 T_{s2}) \cos(k_1 X'_{s1})}{k_1} \right. \\
&\quad \left. - k_{12} \cosh(\delta_1 T_{s1}) \cosh(\delta_2 T_{s2}) \right], \\
H &= -2k_{12} \left[\frac{\delta_1 \delta_2 \sinh(\delta_1 T_{s1}) \cos(k_2 X'_{s2})}{k_2} - \frac{\sinh(\delta_2 T_{s2}) \cos(k_1 X'_{s1}) \delta_2 \delta_1}{k_1} \right. \\
&\quad \left. - \delta_1 \sinh(\delta_1 T_{s1}) \cosh(\delta_2 T_{s2}) + \delta_2 \cosh(\delta_1 T_{s1}) \sinh(\delta_2 T_{s2}) \right], \\
F &= \frac{2(k_1^2 + k_2^2) \delta_1 \delta_2 \cos(k_1 X'_{s1}) \cos(k_2 X'_{s2})}{k_1 k_2} \\
&\quad - (2k_1^2 - k_1^2 k_2^2 + 2k_2^2) \cosh(\delta_1 T_{s1}) \cosh(\delta_2 T_{s2}) \\
&\quad + 4\delta_1 \delta_2 [\sin(k_1 X'_{s1}) \sin(k_2 X'_{s2}) + \sinh(\delta_1 T_{s1}) \sinh(\delta_2 T_{s2})] \\
&\quad - 2k_{12} \left[\frac{\delta_1 \cos(k_1 X'_{s1}) \cosh(\delta_2 T_{s2})}{k_1} - \frac{\delta_2 \cos(k_2 X'_{s2}) \cosh(\delta_1 T_{s1})}{k_2} \right]
\end{aligned}$$

with

$$\begin{aligned}
T_{s1} &= T - T'_0, & T_{s2} &= T - T_0, & X_{sj} &= X - X_j, \\
X'_{s1} &= X_{s1} - vT, & X'_{s2} &= X_{s2} - vT, & \delta_j &= 0.5k_j \sqrt{4 - k_j^2}, \\
k_{12} &= k_1^2 - k_2^2, & k_1 &= 2\sqrt{1 + n_1^2}, & k_2 &= 2\sqrt{1 + n_2^2}.
\end{aligned}$$

Here X and T satisfy Eq. (3), ϕ is given by Eq. (4), v is an arbitrary constant, n_j are complex eigenvalues in DT, T_0 , T'_0 and X_j determine the center of solution in (T, X) coordinates.

For simplicity, we firstly analyze breather solution (7) in the framework of the standard NLSE (5), and the dynamical properties of solution (7) for Eq. (1) will be discussed in the next section. In fact, breather solution (7) in the framework of the standard NLSE (5) is two breathers built from first-order RWs [19], and two kinds of structures is demonstrated in Fig. 1. Figures 1a and 1b show two parallel breathers, whose number of RWs determined by the ratio of k_1 and k_2 . Here we choose $k_1 : k_2 = 2 : 3$, thus the ratio of the numbers of RWs in breathers is also 2 : 3.

In Figs. 1a and 1b, one array of two breathers has different positions in X direction, that is, the centers of breathers at $T = -6$ in Figs. 1a and 1b are same but those at $T = 6$ are different with (a) $X_2 = 5$ and (b) $X_2 = 3$. This difference produces different kinds of superposed RW-like breathers shown in Figs. 1c and 1d when two arrays of breathers share the same origin.

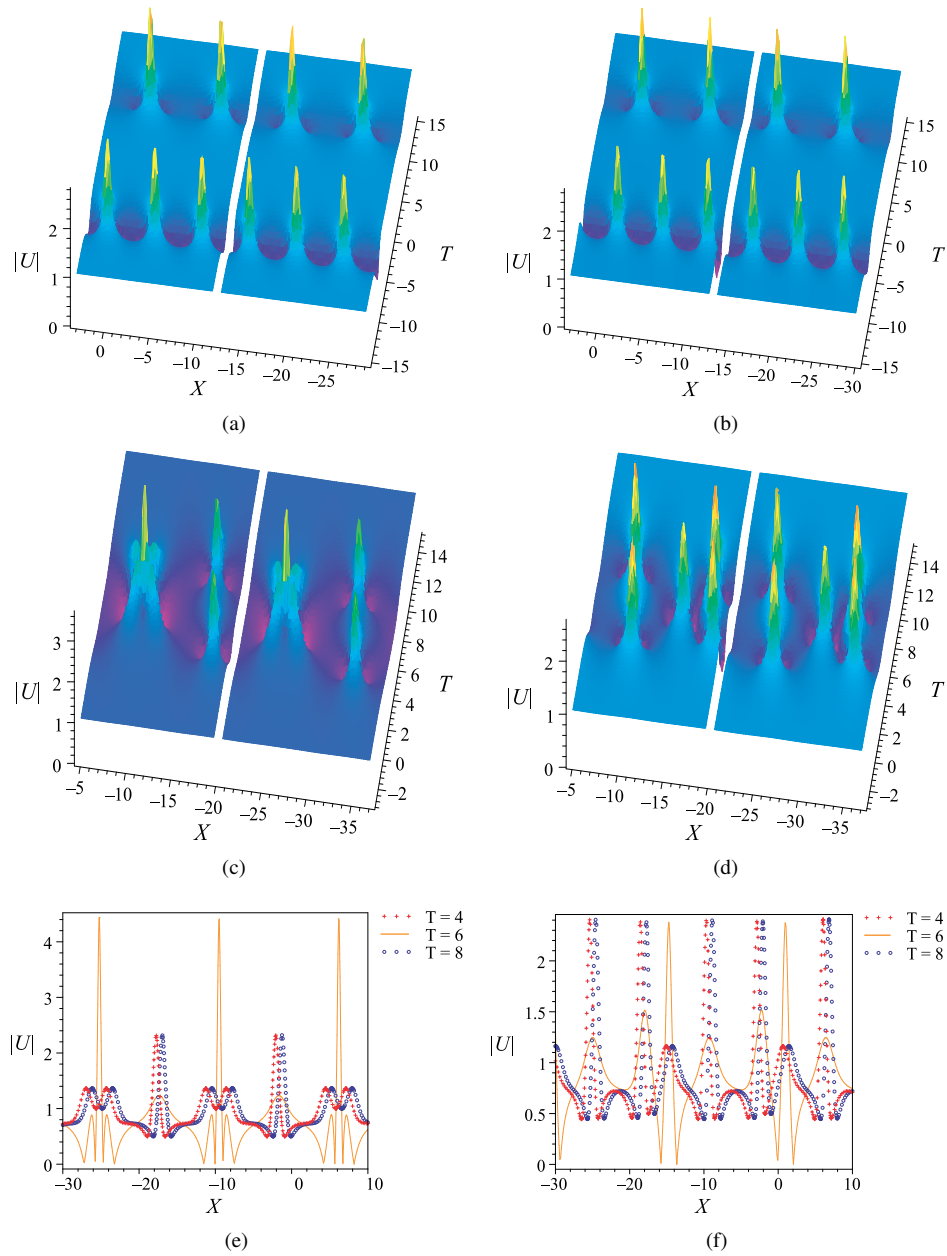


Figure 1. (a) and (b) Two breathers with different positions in T direction; Nonlinear superposition of (c) second-order RWs and first-order RW-pairs and (d) RW triplets and first-order RW-pairs for Eq. (5) in the (T, X) coordinates; (e) and (f) Sectional view at different T corresponding to (c) and (d), respectively. The parameters are chosen as $k_1 = 0.8$, $k_2 = 1.2$, $T_0 = T'_0 = 6$, $v = 0.2$ with (a), (c), (e) $X_1 = X_2 = 5$ and (b), (d), (f) $X_1 = 5$, $X_2 = 3$. For (a) and (b), $T_0 = -6$, $T'_0 = 6$. (Online version in color.)

Next we analyze the conformation from Figs. 1a to 1c and from Figs. 1b to 1d. In Figs. 1a–1d, there are white lines to separate figures into two similar parts. In the left part of Fig. 1a, two RWs near white line possess the same X value, and other three RWs generate a triangular distribution. When five RWs share the same origin (cf. Fig. 1c), two RWs have not overlapped but produced RW-pair, and other three first-order RWs recombine into a second-order RW. Five RWs in the right part of Fig. 1a have similar case. In each part of Fig. 1b, when five RWs share the same origin (cf. Fig. 1d), RW triplets and RW-pair generate respectively. Note that there exists X -directional shift together for RWs during the process of nonlinear superposition. To comprehend these two kinds of superposed RW-like breathers, we show sectional view at different T corresponding to Figs. 1c and 1d in Figs. 1e and 1f.

3 Controllable superposed RW-like breathers

From solution (7), the peak is modulated by $(\sqrt{l_2}/W)\sqrt{\beta/\chi}$, the width $W(t)$ and center position $\xi_c(t)$ are given in (5). The chirp of phase and phase shift are determined by $W_t/(2\beta W)$ and $(3/2)\int_0^t \beta(\tau)b^2(\tau) d\tau$ with linear phase $b(t)$ existing constraint in (3). From these expressions, we know that the diffraction $\beta(t)$, nonlinearity $\chi(t)$ and gain/loss $\gamma(t)$ parameters interplay together to impact evolutionary characteristics such as the amplitude, width, center and phase.

Besides these controllable factors above, a vital factor for the propagation type is the relation (5) between the accumulated time T and the real time t , where the diffraction, nonlinearity and gain/loss coefficients play an important role. In the following, we discuss this kind control for the propagation type in two systems. The first system is the diffraction decreasing medium (DDM) with the Logarithmic profile [5, 17]

$$\begin{bmatrix} \beta(t) \\ \chi(t) \end{bmatrix} = \begin{pmatrix} \beta_0 \\ \chi_0 \end{pmatrix} \ln \left\{ e + \frac{t}{L} \left[\exp\left(\frac{1}{C}\right) - e \right] \right\}, \quad (8)$$

where $1/C$ describes the compression ratio, and L is the setting time in BECs or length of the medium in nonlinear optics with the natural logarithm e , constants β_0 and χ_0 describe initial diffraction and nonlinearity, and the gain/loss parameter $\gamma = \gamma_0$ (const). The second one is a periodic diffraction amplification system (PDAS) [16, 37]

$$\beta(t) = \beta_0 \exp(-\sigma t) \cos(\delta t), \quad \chi = \chi_0 \exp(-\lambda t) \cos(\delta t), \quad (9)$$

where β_0 and χ_0 are the parameters related to the initial diffraction and nonlinearity in system, and σ , λ and δ are the parameters about varying degree of diffraction and nonlinearity. In particular, when $\delta = 0$, Eq. (9) corresponds to the exponentially modulated control parameters [9, 31], which is a typical case in DDM for $\sigma > 0$.

Note that the similarity variable X and the accumulated time T are not real spatial and time variables x , y , z , t . Specially, from Eq. (4), choosing different diffraction and nonlinearity coefficient, different dynamical behaviors for superposed RW-like breathers

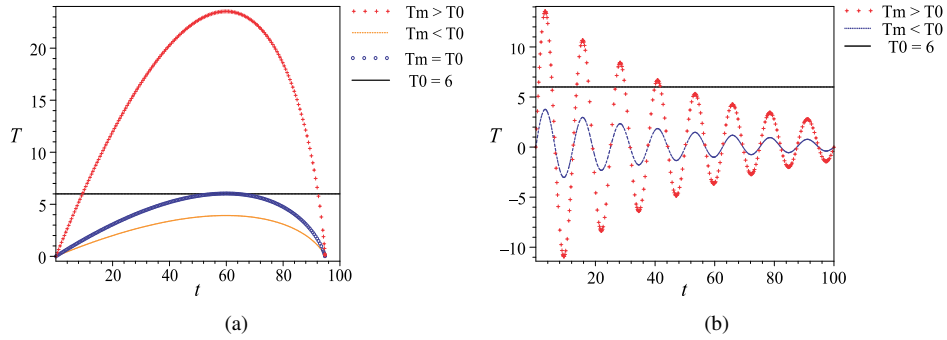


Figure 2. Comparison between the maximum accumulated time T_m and the accumulated time T_0 with the center of RWs in the (a) Logarithmic and (b) PDAS. Parameters are chosen as (a) $\chi_0 = 0.5$, $p = r = 0.1$, $q = 0.2$, $L = 50$, $C = 4$ with $\beta_0 = 0.2$ (red cross), 0.78 (blue circle) and 1.2 (gold dash); and (b) $\chi_0 = \delta = 0.5$, $\sigma = 0.1$, $\lambda = 0.05$, $\gamma_0 = -0.005$, $p = 0.5$, $q = 0.4$, $r = 0.6$ with $\beta_0 = 0.25$ (red cross) and 0.9 (blue dash). (Online version in color.)

in Fig. 1 will appear. Figure 2 exhibits the integral relation between T and t in Logarithmic DDM (8) and PDAS (9). Two different systems have a common property, that is, the accumulated time T exists a maximum value T_m . In the framework of Eq. (5), T can choose arbitrary values and breathers reach their maximum amplitudes at $T = T_0$ and then disappear. Therefore, we can adjust the relation between T_m and T_0 to realize the control for superposed breathers.

In the Logarithmic DDM (8), from the second expression in Eq. (3), the accumulated time T has the relation to time t with $T = 9(p^2 + q^2 + r^2)\chi_0^2\{1 - \ln[(te^{1/C} + (L-t)e)/L]\}\{eL/[e - e^{1/C}] - t\}/\beta_0$, which indicates that T exists a maximal value T_m (see Fig. 2a). When $t = L(e-1)/(e - e^{1/C})$, $T \rightarrow T_m = (p^2 + q^2 + r^2)\chi_0^2 L/[\beta_0(e - e^{1/C})]$. The propagation behaviors of breather are controlled by modulating the relation between T_m and T_0 .

When T_m is remarkably bigger than T_0 (see the red cross in Fig. 2a), the full second-order RWs and first-order RW-pairs are excited quickly (cf. Figs. 3a and 1c). The pattern at a trap in (x, y) plane is shown in Fig. 3b, where the trap from Eq. (6) slopes from the upper left to bottom-right corner. If $T_m = T_0$, second-order RWs in breathers can maintain a long time, and their amplitude and width self-similarly vary (cf. Fig. 3c). Moreover, a RW in first-order RW-pair also sustain its shape but another disappears. At last, if $T_m < T_0$, wave in the framework of Eq. (1) have not sufficient time to excite second-order RWs, and restraint of second-order RWs will happen (cf. Fig. 3d). Only part of second-order RWs and one RW in first-order RW-pair are produced, and another in first-order RW-pair is annihilated.

For another kind of superposed breather in Fig. 1d, there are some similar results. When T_m is notably bigger than T_0 (see the red cross in Fig. 2a), the full RW triplets and first-order RW-pairs are excited quickly (cf. Figs. 4a and 1d). The pattern at a trap in (x, y) plane is shown in Fig. 4b, where the trap is same as that in Fig. 3b. If $T_m = T_0$, two RWs in triplets and one RW in first-order RW-pair maintain a long lasting time in

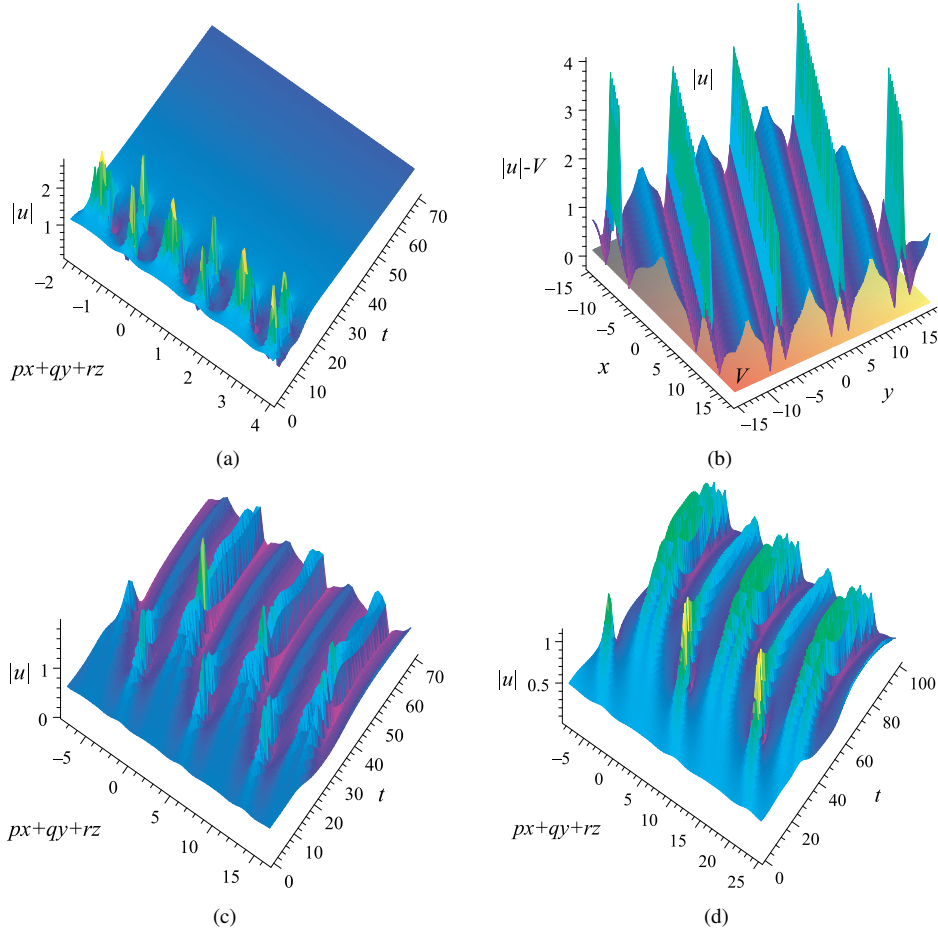


Figure 3. (a) Fast excitation, (c) maintenance and (d) restraint of self-similar RW-like breathers in Fig. 1a in the Logarithmic DDM, (b) quickly excited RW-like breathers corresponding to (a) in a trap at $t = 9.5$, $z = 2$ in (x, y) coordinates. Parameters in (a), (c) and (d) correspond to $\beta_0 = 0.2$ (red cross), $\beta_0 = 0.78$ (blue circle) and $\beta_0 = 1.2$ (gold dash) in Fig. 2a. Other parameters are chosen as $b_0 = 0.5$, $\gamma_0 = -0.005$. (Online version in color.)

a self-similar manner but one RW in triplets and one RW in RW-pair both annihilate. At last, if $T_m < T_0$, the threshold of exciting triplets and pairs are both never reached and the excitations of them are both restrained (cf. Fig. 4d). Only part of superposed RW-like breather is produced.

Different from the controllable behaviors in the Logarithmic DDM (8), breather in the PDAS (9) can happen recurrence behavior. In the PDAS (9), from the second expression in Eq. (3), we have

$$T = \frac{9(p^2 + q^2 + r^2)\chi_0^2\{\Delta[\delta \sin(\delta t) - \Delta \sin(\delta t)] \exp(-\Delta t)\}}{\beta_0[4(2\gamma_0 - \lambda)(\sigma - \lambda + 2\gamma_0)] + \sigma^2 + \delta^2}$$

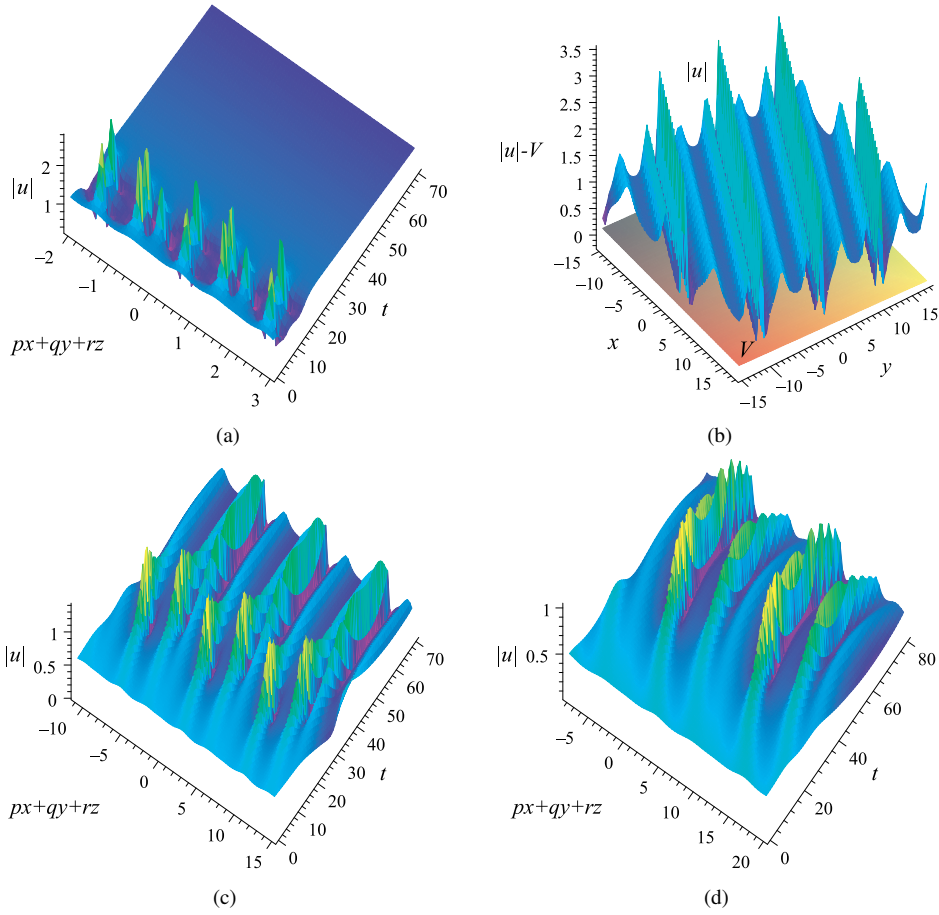


Figure 4. (a)–(d) all cases are corresponding to Fig. 3 except for this control to breathers in Fig. 1b. (Online version in color.)

with $\Delta = 2\lambda - 4\gamma_0 - \sigma$. This relation indicates that T changes within the domain

$$|T| \leq T_{\max} = \frac{9(p^2 + q^2 + r^2)\chi_0^2\{\Delta + \delta \exp[-\Delta\pi/(2\delta)]\}}{\beta_0[4(2\gamma_0 - \lambda)(\sigma - \lambda + 2\gamma_0)] + \sigma^2 + \delta^2}.$$

Thus, as shown in Fig. 2b, the value of T decreases periodically with oscillating behavior and the maximum T_m appears in the first period. This periodic change of T can produce recurrence of breather.

Here we discuss two different cases: $T_m > T_0$ and $T_m < T_0$. For these two different cases, breathers will demonstrate different dynamical behaviors, and can realize the dynamical manipulation. This controllability for breather in the PDAS (9) is remarkably different from that in the Logarithmic DDM. For breather in Fig. 1c, when $T_m > T_0$ (red

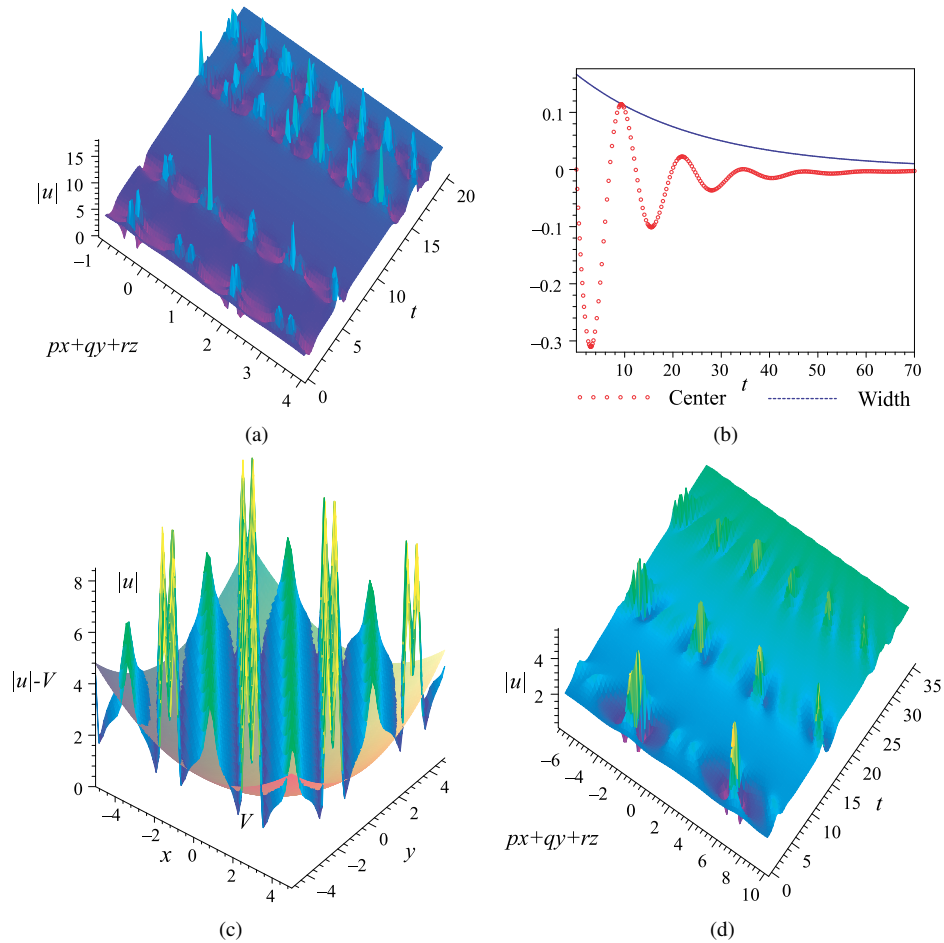


Figure 5. (a) Recurrence and (d) restraint of RW-like breathers in Fig. 1a in the PDAS, (b) the evolution of center and width for breather, and (c) RW-like breather corresponding to (a) in a trap at $t = 5.6$, $z = 2$ in (x, y) coordinates. Parameters in (a) and (d) correspond to $\beta_0 = 0.25$ (red cross) and 0.9 (blue dash) in Fig. 2b with $b_0 = 0.5$. (Online version in color.)

cross in Fig. 2b), breather will recur periodically (cf. Fig. 5a). It exhibits this recurred behavior of breather in detail, the gap between second-order RWs and first-order RW-pairs decreases, and RWs become concentrated with the increase of time t . Fig. 5b shows the evolution of center and width for breather. The center oscillates some periods and gradually tends to a fixed value, and width decreases by degrees when t adds. Different from Figs. 3b and 4b, there is a parabolic trap from Eq. (6) in Fig. 5c, where the layout of second-order RWs and first-order RW-pairs appears in (x, y) plane under the action of this trap. If $T_m < T_0$, wave in the framework of Eq. (1) have not sufficient time to be excited. As shown in Fig. 5d, second-order RWs are completely restrained, and only initial M-shaped part are produced. Moreover, RW-pairs are also only excited to one RW.

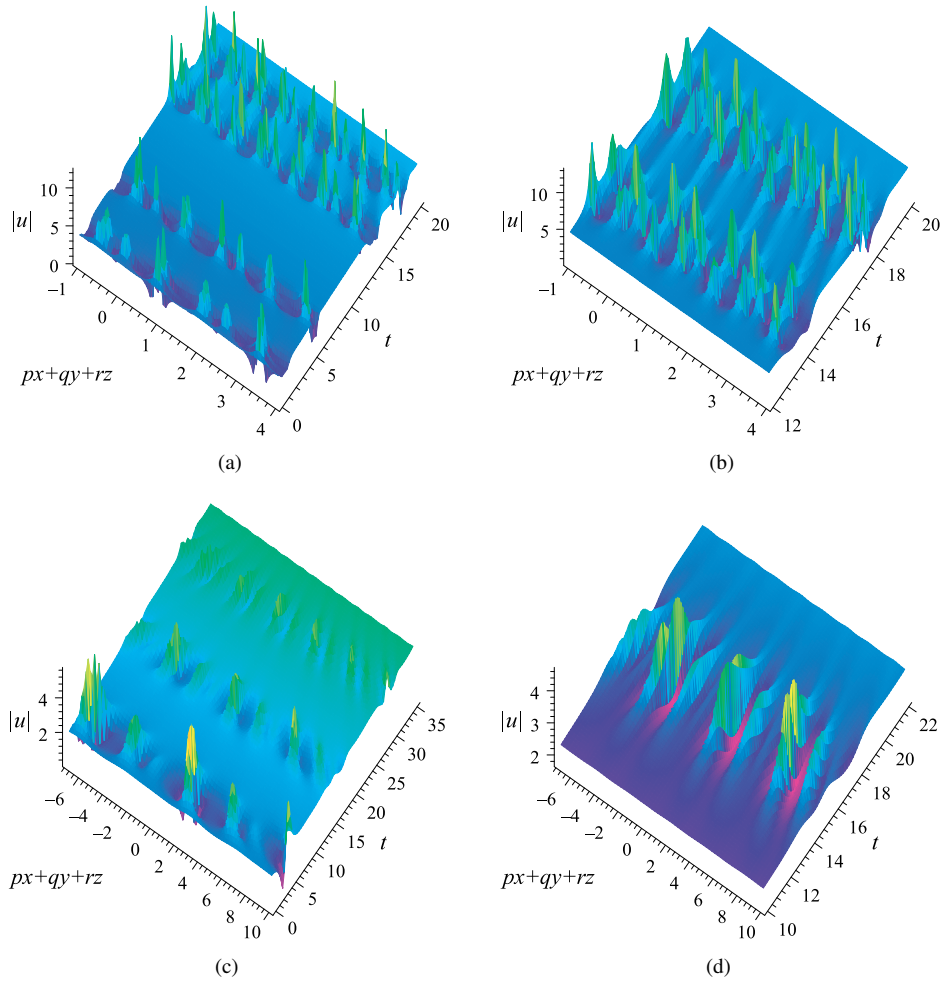


Figure 6. (a) Recurrence and (c) restraint of self-similar RW-like breathers in Fig. 1b in the PDAS, (b) and (d) different domain views for (a) and (c), respectively. Parameters are same as Fig. 5. (Online version in color.)

Similarly, when t adds, restrained superposed breather becomes concentrated, and its amplitude dies out quickly.

Similar cases happen for the second kind of superposed breather. When $T_m > T_0$, breather also recurs periodically in Fig. 6a. From the enlarged plot in Fig. 6b, RW triplets and pairs both periodically appear, and the space between them gradually reduces. When $T_m < T_0$, the threshold of exciting full triplets and pairs are both never reached and the excitations of them are both restrained. Only one RW in RW-pairs is excited (cf. Fig. 6c and Fig. 1d). From the enlarged plot in Fig. 6d, RWs in breather are remarkably restrained when t adds.

4 Stability and possible observation

The stability of analytical solutions is important in the realistic application, namely, how they evolve with time when they are disturbed from their analytically given forms. We perform direct numerical simulations with initial white noise for Eq. (1) using split-step pulse propagation method, with initial fields coming from Eq. (7) in DDM and PDAS. Numerical calculations show no collapse. Instead, stable propagation with a long time is observed. Two examples of such behaviors are displayed in Fig. 7, which essentially presents a numerical rerun of Figs. 3c and 5a.

Moreover, we consider the comparison between 1D and 3D cases. Note that the transition from 3D to 1D NLSE is well established in nonlinear optics and BECs [27]. Solutions are similar to (7) except for the width $W_{1D} = \beta/(\chi \exp(2\Gamma))$ from the calculation for 1D case of Eq. (1). From Fig. 7, the 1D case is stable and has smaller period along x -axis than 3D case, and the amplitude's oscillation in parts between RWs in 3D case is more severe than that in 1D case. The white noise has more obviously impact for 3D case in DDM than that in PDAS.

This difference for stability implies that 3D breather is observed more difficult than 1D case. In nonlinear optics, Dudley et al. [14] observed breather in the experiment by putting the initial 1ns pulse at 1064 nm with the power $P_0 = 43$ W into fiber with parameters $\beta = -75$ ps²km⁻¹, $\chi = 60$ W⁻¹km⁻¹. However, waves here carry infinite energy because $\int_{-\infty}^{+\infty} |u(x, y, z, t)|^2 dx dy dz$ diverges. Thus an aperture at the source plane is required to observe the proposed solutions in a laboratory. Similar to method for realizing linear optical bullets [30], we use the envelope of u_0 in the source plane in the form $u_0 = \Theta(L_x - |x|)\Theta(L_y - |y|)u(px + qy + rz)$, where $\Theta(\zeta)$ is a unit step-function, $2L_x$ and $2L_y$ are the dimensions of the source aperture. The Fourier transform and inverse transform with the Fresnel diffraction theory make a finite aperture do not significantly affect their intensity profiles of idealized (infinite-energy) breathers. Thus, we can use this experimental protocol to create breathers here.

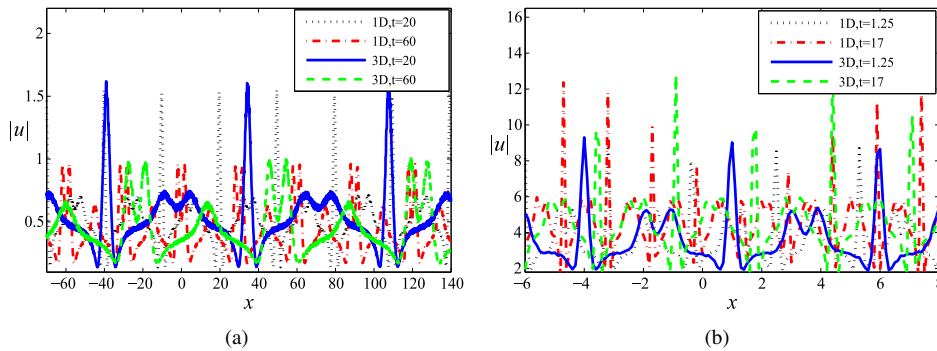


Figure 7. Comparison of stability between 1D and 3D cases: (a) maintenance for Figs. 3c and 3b recurrence corresponding to Fig. 5a. Only the dependence on x is shown for 3D case. An added 5% white noise are added to the initial values. (Online version in color.)

5 Conclusions

In short, we review the main points offered in this paper:

- Spatiotemporal superposed breather solution built from first-order and second-order RWs are obtained.
3D vcNLSE with linear and parabolic potentials is investigated. A relation between this equation and the standard NLSE is found, and exact spatiotemporal breather solution is obtained. Superposed breathers are constructed when two parallel breathers with different numbers of RWs, decided by ratio of k_1 and k_2 , share the origin. When choosing $k_1 : k_2 = 2 : 3$, two kinds of superposed RW-like breathers are constructed, that is, breathers constructed by second-order RWs or RW triplets and first-order RW-pairs.
- Controllable behaviors of these breathers in different systems can be studied by modulating the relation between the maximum accumulated time T_m from the integral relation and the accumulated time T_0 with the center of RW-like breathers. These results are listed in Table 1. We also give an experimental protocol to observe these phenomena in future experiments.

Table 1. Controllable behaviors in different systems.

—	Logarithmic DDM	Periodic system
$T_m > T_0$	Fast excitation	Recurrence
$T_m = T_0$	Maintenance	—
$T_m < T_0$	Restraint	Restraint

These results add to our comprehension on the manipulation for breather, and stimulate novel experiments in the context of the optical communications, plasma physics and Bose–Einstein condensations, and so on.

References

1. N. Akhmediev, J.M. Soto-Crespo, A. Ankiewicz, Extreme waves that appear from nowhere: On the nature of rogue waves, *Phys. Lett. A*, **373**:2137–2145, 2009.
2. N. Akhmediev, J.M. Soto-Crespo, A. Ankiewicz, How to excite a rogue wave, *Phys. Rev. A*, **80**, 043818, 2009.
3. A. Ankiewicz, J.M. Soto-Crespo, N. Akhmediev, Rogue waves and rational solutions of the Hirota equation, *Phys. Rev. E*, **81**, 046602, 2010.
4. A. Chabchoub, N.P. Hoffmann, N. Akhmediev, Observation of rogue wave in a water wave tank, *Phys. Rev. Lett.*, **106**, 204502, 2011.
5. M.G. Da Silva, K.Z. Nobrega, A.S.B. Sombra, Analysis of soliton switching in dispersion-decreasing fiber couplers, *Opt. Commun.*, **171**:351–364, 1999.
6. C.Q. Dai, C.Y. Liu, Solitary wave fission and fusion in the $(2 + 1)$ -dimensional generalized Broer–Kaup system, *Nonlinear Anal. Model. Control*, **17**:271–279, 2012.

7. C.Q. Dai, Q. Tian, S.Q. Zhu, Controllable behaviours of rogue wave triplets in the nonautonomous nonlinear and dispersive system, *J. Phys. B, At. Mol. Opt. Phys.*, **45**, 085401, 2012.
8. C.Q. Dai, Y.Y. Wang, Q. Tian, J.F. Zhang, The management and containment of self-similar rogue waves in the inhomogeneous nonlinear Schrödinger equation, *Ann. Phys.*, **327**:512-521, 2012.
9. C.Q. Dai, Y.Y. Wang, X.G. Wang, Ultrashort self-similar solutions of the cubic-quintic nonlinear Schrödinger equation with distributed coefficients in the inhomogeneous fiber, *J. Phys. A, Math. Theor.*, **44**, 155203, 2011.
10. C.Q. Dai, Y.Y. Wang, J.F. Zhang, Analytical spatiotemporal localizations for the generalized $(3 + 1)$ -dimensional nonlinear Schrödinger equation, *Opt. Lett.*, **35**:1437–1439, 2010.
11. C.Q. Dai, X.G. Wang, G.Q. Zhou, Stable light-bullet solutions in the harmonic and parity-time-symmetric potentials, *Phys. Rev. A*, **89**, 013834, 2014.
12. C.Q. Dai, J.F. Zhang, Controllable dynamical behaviors for spatiotemporal bright solitons on continuous wave background, *Nonlinear Dyn.*, **73**:2049–2057, 2013.
13. C.Q. Dai, G.Q. Zhou, J.F. Zhang, Controllable optical rogue waves in the femtosecond regime, *Phys. Rev. E*, **85**, 016603, 2012.
14. J.M. Dudley, G. Genty, F. Dias, B. Kibler, N. Akhmediev, Modulation instability, Akhmediev Breathers and continuous wave supercontinuum generation, *Opt. Express*, **17**, 21497, 2009.
15. J.M. Dudley, G. Genty, B.J. Eggleton, Harnessing and control of optical rogue waves in supercontinuum generation, *Opt. Express*, **36**:3644–3651, 2008.
16. R. Ganapathy, Soliton dispersion management in nonlinear optical fibers, *Commun. Nonlinear Sci. Numer. Simul.*, **17**:4544-4550, 2012.
17. R. Ganapathy, V.C. Kuriakose, Soliton pulse compression in a dispersion decreasing elliptic birefringent fiber with effective gain and effective phase modulation, *J. Nonlinear Opt. Phys. Mater.*, **11**, 185–195, 2002.
18. N. Karjanto, E. van Groesen, Qualitative comparisons of experimental results on deterministic freak wave generation based on modulational instability, *J. Hydro-Environ. Res.*, **3**:186–192, 2010.
19. D.J. Kedziora, A. Ankiewicz, N. Akhmediev, Second-order nonlinear Schrödinger equation breather solutions in the degenerate and rogue wave limits, *Phys. Rev. E*, **85**, 066601, 2012.
20. B. Kibler, J. Fatome, C. Finot, G. Millot, F. Dias, G. Genty, N. Akhmediev, J.M. Dudley, The Peregrine soliton in nonlinear fibre optics, *Nat. Phys.*, **6**:790–795, 2010.
21. J.C. Liang, H.P. Liu, F. Liu, L. Yi, Analytical solutions to the $(3 + 1)$ -dimensional generalized nonlinear Schrödinger equation with varying parameters, *J. Phys. A, Math. Theor.*, **42**, 335204, 2009.
22. Z.Y. Ma, S.H. Ma, Analytical solutions and rogue waves in $(3 + 1)$ -dimensional nonlinear Schrödinger equation, *Chin. Phys. B*, **21**, 030507, 2012.
23. B.A. Malomed, *Soliton Management in Periodic Systems*, Springer, New York, 2006.

24. R. Morris, A.H. Kara, A. Biswas, Soliton solution and conservation laws of the Zakharov equation in plasmas with power law nonlinearity, *Nonlinear Anal. Model. Control*, **18**:153–159, 2013.
25. A. Osborne, M. Onorato, M. Serio, The nonlinear dynamics of rogue waves and holes in deep-water gravity wave train, *Phys. Lett. A*, **275**:386–393, 2000.
26. D.H. Peregrine, Water waves, nonlinear Schrödinger equations and their solutions, *J. Aust. Math. Soc., Ser. B*, **25**:16–43, 1983.
27. C.J. Pethick, H. Smith, *Bose–Einstein Condensation in Dilute Gases*, Cambridge University Press, Cambridge, 2002.
28. N.Z. Petrović, M. Belić, W.P. Zhong, Spatiotemporal wave and soliton solutions to the generalized $(3 + 1)$ -dimensional Gross–Pitaevskii equation, *Phys. Rev. E*, **81**, 016610, 2010.
29. N.Z. Petrović, H. Zahreddine, M. Belić, Exact spatiotemporal wave and soliton solutions to the generalized $(3 + 1)$ -dimensional nonlinear Schrödinger equation with linear potential, *Phys. Scr.*, **83**, 065001, 2011.
30. S.A. Ponomarenko, G.P. Agrawal, Linear optical bullets, *Opt. Commun.*, **261**:1–4, 2006.
31. M.S. Rajan Mani, A. Mahalingam, A. Uthayakumar, K. Porsezian, Observation of two soliton propagation in an erbium doped inhomogeneous lossy fiber with phase modulation, *Commun. Nonlinear Sci. Numer. Simul.*, **18**:1410–1432, 2013.
32. D.R. Solli, C. Ropers, P. Koonath, B. Jalali, Optical rogue waves, *Nature*, **450**:1054–1057, 2007.
33. Y.Y. Wang, J.T. Li, C.Q. Dai, X.F. Chen, J.F. Zhang, Solitary waves and rogue waves in a plasma with nonthermal electrons featuring Tsallis distribution, *Phys. Lett. A*, **377**:2097–2104, 2013.
34. X.F. Wu, G.S. Hua, Z.Y. Ma, Novel rogue waves in an inhomogeneous nonlinear medium with external potentials, *Commun. Nonlinear Sci. Numer. Simul.*, **18**:3325–3336, 2013.
35. Z.Y. Yan, V.V. Konotop, N. Akhmediev, Three-dimensional rogue waves in nonstationary parabolic potentials, *Phys. Rev. E*, **82**, 036610, 2010.
36. W.P. Zhong, M.R. Belić, T.W. Huang, Two-dimensional accessible solitons in PT-symmetric potentials, *Nonlinear Dyn.*, **70**:2027–2034, 2012.
37. H.P. Zhu, Nonlinear tunneling for controllable rogue waves in two dimensional graded-index waveguides, *Nonlinear Dyn.*, **72**:873–882, 2013.